Nanoscale

PAPER

View Article Online
View Journal | View Issue

Cite this: *Nanoscale*, 2021, **13**, 218

Local administration of stem cell-derived extracellular vesicles in a thermoresponsive hydrogel promotes a pro-healing effect in a rat model of colo-cutaneous post-surgical fistula†

Arthur Berger,[a] Irami Araújo-Filho,[b] Max Piffoux,[c,d,e] Alba Nicolás-Boluda,[c] Alice Grangier,[c] Imane Boucenna,[c] Caroline Cristiano Real,[f] Fabio Luiz Navarro Marques,[f] Daniele de Paula Faria,[f] Amália Cinthia Meneses do Rego,[g] Chloe Broudin,[h] Florence Gazeau,[c] Claire Wilhelm,[c] Olivier Clément,[i] Christophe Cellier,[j] Carlos Alberto Buchpiguel,[f] Gabriel Rahmi*‡[a,j] and Amanda K. A. Silva*‡[c]

Extracellular vesicles (EVs), especially from stem/stromal cells (SCs), represent a cell-free alternative in regenerative medicine holding promises to promote tissue healing while providing safety and logistic advantages in comparison to cellular counterparts. Herein, we hypothesize that SC EVs, administered locally in a thermoresponsive gel, is a therapeutic strategy for managing post-surgical colo-cutaneous fistulas. This disease is a neglected and challenging condition associated to low remission rates and high refractoriness. Herein, EVs from a murine SC line were produced by a high-yield scalable method in bioreactors. The post-surgical intestinal fistula model was induced *via* a surgical cecostomy communicating the cecum and the skin in Wistar rats. Animals were treated just after cecostomy with PBS, thermoresponsive Pluronic F-127 hydrogel alone or containing SC EVs. A PET-monitored biodistribution investigation of SC EVs labelled with ^{89}Zr was performed. Fistula external orifice and output assessment, probe-based confocal laser endomicroscopy, MRI and histology were carried out for therapy follow-up. The relevance of percutaneous EV administration embedded in the hydrogel vehicle was indicated by the PET-biodistribution study. Local administration of SC EVs in the hydrogel reduced colo-cutaneous fistula diameter, output, fibrosis and inflammation while increasing the density of neo-vessels when compared to the PBS and gel groups. This multi-modal investigation pointed-out the therapeutic potential of SC EVs administered locally and in a thermoresponsive hydrogel for the management of challenging post-surgical colon fistulas in a minimally-invasive cell-free strategy.

Received 14th October 2020,
Accepted 23rd November 2020

DOI: 10.1039/d0nr07349k

rsc.li/nanoscale

Introduction

Extracellular vesicles (EVs) from stem/stromal cells (SCs) are recent players in the evolving landscape of regenerative medicine bringing along new promises and challenges. In the frontline of cell therapy, SCs are known to provide the microenvironment with trophic and survival signals including cytokines released by means of EVs, pointing out EV role in paracrine

[a]*Laboratoire Imagerie de l'Angiogénèse, Plateforme d'Imagerie du Petit Animal, PARCC, INSERM U970, Université de Paris, 75015 Paris, France. E-mail: gabriel.rahmi@aphp.fr*
[b]*Universidade Federal do Rio Grande do Norte, Hospital Universitário Onofre Lopes, 59.012-300 Natal – RN, Brazil*
[c]*Laboratoire Matière et Systèmes Complexes (MSC), Université de Paris, UMR 7057 CNRS, 75205 Paris Cedex 13, France. E-mail: amanda.silva@univ-paris-diderot.fr*
[d]*Department of Medical Oncology, Centre Léon Bérard, 69008 Lyon, France*
[e]*INSERM UMR 1197 – Interaction cellules souches-niches: physiologie, tumeurs et réparation tissulaire, Hôpital Paul-Brousse, 94807 Villejuif Cedex, France*
[f]*Laboratory of Nuclear Medicine (LIM-43), Departamento de Radiologia e Oncologia, Faculdade de Medicina, Universidade de Sao Paulo, 05403-911 Sao Paulo, Brazil*
[g]*Liga Norte Riograndense Contra o Câncer, 59075-740 Natal – RN, Brazil*
[h]*Hôpital Européen Georges Pompidou, Department of Pathology, Assistance Publique des Hôpitaux de Paris, Université de Paris, 75015 Paris, France*
[i]*Department of Radiology, Hôpital Européen Georges Pompidou, Assistance Publique des Hôpitaux de Paris, 75015 Paris, France*
[j]*Gastro-Enteroloy and Endoscopy Department, Hôpital Européen Georges Pompidou, Assistance Publique des Hôpitaux de Paris, Université de Paris, 75015 Paris, France*
†Electronic supplementary information (ESI) available: ESI figures. See DOI: 10.1039/d0nr07349k
‡These authors equally contributed to this work.

effect.[1,2] EVs, including exosomes, microvesicles and apoptotic bodies, are sub-cellular membrane-enclosed entities at the nanometer size range (40–5000 nm diameter) shed by cells either in a constitutive or in an inducible basis.[3–5] Pleiotropic effects have been reported for SC EVs, such as the (i) induction of pro-angiogenesis;[6] (ii) inhibition of cell apoptosis;[7,8] (iii) cell proliferation promotion;[9] (iv) inflammation reduction[10] and (v) fibrosis attenuation.[10–12] For instance, SC EVs have been shown to induce proliferation and apoptosis resistance in a rat model of renal ischemia/reperfusion injury[13] and in a rat model of hepatectomy.[11] SC-derived EVs also reduced infarct size in a mouse model of myocardial ischemia/reperfusion, mediating a cardioprotective effect.[2] The regenerative properties of SC EVs were also reported for cutaneous wounds,[14,15] bone fracture[16] as well as for brain[6] and lung injuries.[10] The current body of evidence on EV regenerative properties gave rise to a paradigm shift, switching cell therapy to sub-cellular (EV) therapy. The strength of EV therapy is the perspective to mitigate risks of uncontrolled cell replication, differentiation or vascular occlusion, offering storage and shelf-life gains.[17,18] Another key asset is the immune-privileged status of SC EVs allowing to consider an allogeneic setting[17] as an "off-the-shelf" therapeutic modality.[19,20]

Going beyond the assets, the other side of the coin concerns the challenges for rendering EV-based regenerative medicine clinically feasible. In this regard, there is namely the demand for high-yield, cost-effective, scalable and standardized EV production complying with regulatory issues and compatible with good manufacturing practice (cGMP) requirements. Another challenge is EV administration. Systemically administered EVs have a short half-life with a rapid uptake by the mononuclear phagocyte system especially in the liver and spleen.[21–23] This points out the importance of local rather than systemic administration to improve EV retention in the site of interest.[24,25] EV combination to a biomaterial may represent an eligible strategy in the attempt to extend EV residence time in the target and modulate EV release.[26,27] In this regard, injectable hydrogels offer the advantages of filling irregular defects and reaching low-accessible areas while enabling the possibility to tune release profile depending on the material choice.[28] Thermoresponsive hydrogels that exhibit a lower critical solution temperature (Pluronic F-127 (PF-127), poly (*N*-isopropylacrylamide)) provide the additional advantage of minimally-invasive injection in the liquid state and gelation *in situ* at body temperature, preventing therapy leaking, promoting controlled release and favoring retention at the site of interest.[29,30]

In the present paper, we tackle EV production and administration challenges by testing, respectively, (i) a high-yield scalable cGMP approach for EV production based on a turbulence-induced stimulation directly in bioreactors and (ii) a local thermo-controlled EV delivery in a thermoresponsive hydrogel. In order to test this approach, we address herein unmet needs in the therapy of post-surgical intestinal fistulas, which are abnormal communication between two organs or organ connection to the skin. Digestive fistulas are challenging conditions associated to low remission rates, high morbidity and refractoriness.[31–33] Pharmacological approaches based on the systemic administration of antibiotics, somatostatin, and immune-modulators result in poor therapeutic outcome.[34–36] More than 75% of the digestive fistula cases are related to a postoperative complication.[37] Post-surgical fistulas are potentially life-threatening mainly due to septic or hemorrhagic complications and are associated to high morbidity.[38] In the USA, complications related to gastrointestinal post-surgical fistulas results in additional length of stay and hospital costs of 7.3 days and $24 129 per patient, respectively, only considering the first hospitalization.[39] The risk of such post-surgical complications in patients undergoing upper gastro-intestinal surgery, for instance, sleeve gastrectomy ranges between 0.5% and 7% (2.5% being considered the overall rate).[40] Colorectal complications related to post-surgical fistulas occur in 3%–11% of cases (6% being considered the overall rate).[41–43] The surgical, endoscopic and radiological management has clearly redesigned and improved the management of these fistulas. Fistula care is provided by a team including surgeons, nurses, enterostomal therapists, social workers and nutritionists who will personalize a treatment plan. Patients without life-threatening complications will receive conservative treatment with local management of fistula output, replacement of fluid and electrolyte losses, nutritional support and antibiotic therapy.[44] Complementarily, endoscopic treatments, with stents or clips have been used.[45] Rescue surgery is required when minimally invasive strategies fail or in case of life-threatening complications.[38] This complex surgery will attempt to close the fistula and reconnect the gastrointestinal tract with a risk of mutilating ileostomy or colostomy. Rescue surgery results in increased morbidity and high mortality rate as well as prolonged hospitalization.[46] Unmet needs in post-surgical fistulas therapy recently motivated the investigation of cell therapy as alternative. In 2018, the European Commission approved Alofisel® for Crohn's disease fistula indication becoming the first allogeneic SC therapy (based on adipose tissue-derived SCs – AdSCs), in Europe to receive marketing authorization approval.[47,48] Although post-surgical fistulas were not listed as a therapeutic indication for Alofisel®, some papers have reported encouraging pre-clinical data based on the administration of AdSCs, associated or not with a biomaterial, for the management of digestive post-surgical complications.[49–51] A clinical trial on AdSC therapy for gastrointestinal post-surgical fistulas is ongoing by the Mayo Clinic (ClinicalTrials.gov identifier: NCT02807389). In this clinical investigation, cells are administered locally using a synthetic prosthesis biomaterial composed of polymers (polyglycolic acid/trimethylene carbonate) that are gradually absorbed by the body.

The aim of this paper is to investigate a biomaterial-based cell-free alternative to post-surgical fistulas. Our approach relies on turbulence SC EVs embedded in a PF-127 thermoresponsive hydrogel administered percutaneously in colocutaneous fistulas (Fig. 1). The relevance of this approach in terms of biodistribution and therapeutic outcome were evaluated.

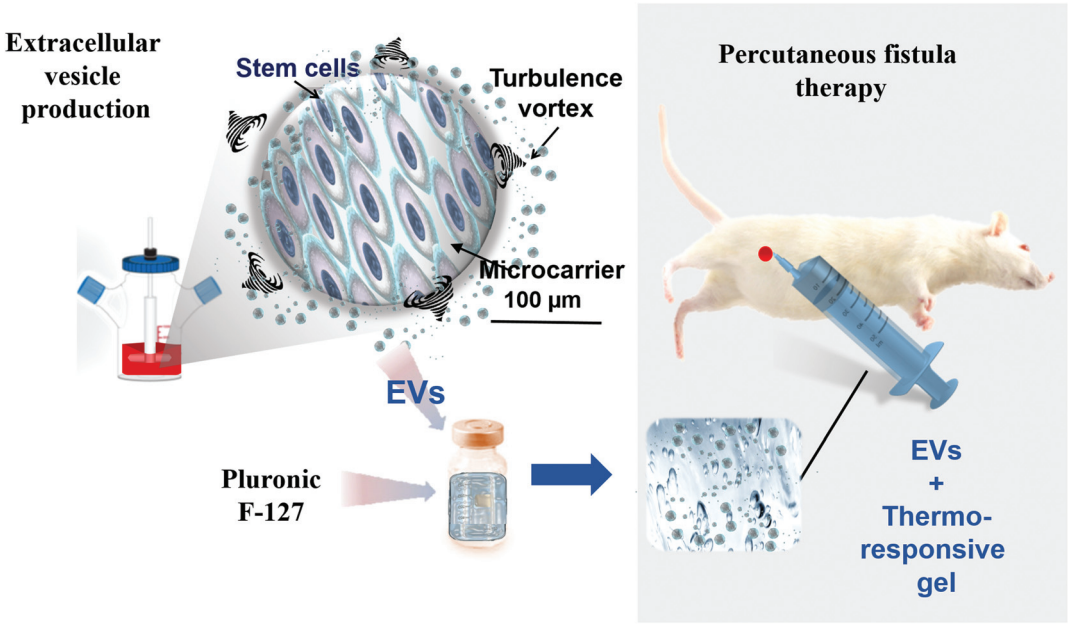

Fig. 1 Schematic representation of the experimental approach based on the production of EVs at high yield by turbulence stimulation from murine stem cells cultured on microcarriers in 1 L bioreactors. EVs were combined to Pluronic F-127 thermoresponsive hydrogel and administered percutaneously at <19 °C (below gel transition temperature) in a colo-cutaneous fistula model in rats. The formulation gelling *in situ* at body temperature is intended to increase EV residence time at the site of interest.

Experimental section

EVs and gel production and characterization

Cell culture in 2D flasks. Murine C3H/10T1/2, Clone 8 (ATCC®) cells were cultured at 37 °C and 5% CO_2. Dulbecco's Modified Eagle Medium (DMEM) supplemented with 10% fetal bovine serum (FBS) and 100 U mL^{-1} penicillin and 100 U mL^{-1} streptomycin was used. Cells were cultured in 150 cm^2 flasks until confluence.

3D cell culture in spinner flask bioreactors. Commercial dextran microcarriers of about 200 µm (Cytodex 1, GE Healthcare) were dispersed in PBS, and autoclaved for sterility. PBS was changed to DMEM without phenol red, and stored at 4 °C. Previous to cell seeding, microcarriers were incubated in 37 °C complete medium at a 6 g L^{-1} concentration during 3 h. Cells were seeded with a cell to microcarrier ratio of 5/1 and submitted to 24 cycles of 45 min of rest followed by 3 min of a gentle mixing at 60 rotations per minute (rpm) in 1 L bioreactor to enable homogeneous adhesion of cells on microcarriers. After cell adhesion, microcarriers were diluted to 3 g L^{-1} with complete medium at 37 °C at 60 RPM until reaching confluence on microcarriers (about 7 days). Every 2–3 days, 30 to 70% of the medium was changed according to the cell confluence.

Turbulence-triggered EV production in spinner flask bioreactors. Once cells were confluent on microcarriers, turbulence-triggered EV production was launched. The protocol consisted in changing the complete medium to heated (37 °C) serum-free DMEM media without phenol red with 100 U mL^{-1} penicillin and 100 U mL^{-1} streptomycin after 3 rinsing steps. By controlling the spinner flask stirring, cells on microcarriers were submitted to a turbulent flow featuring a Kolmogorov length of 35 µm during 4 hours to stimulate EV release.[52] After that, cellular debris of the supernatant were removed by centrifugation at 2000*g* for 10 min. The supernatant was ultracentrifuged at 110 000*g* for 70 min to obtain an EV pellet.

Nanoparticle tracking analysis. EV size distribution and concentration were determined by nanoparticle tracking analysis (NTA) using a Nanosight LM10-HS (NanoSight, UK) with a 405 nm laser. Before measurements, EVs were diluted to an appropriate concentration (between 3×10^8 and 2×10^9 particles per mL) with sterile PBS (confirmed to be particle-free by NTA measurement). For each sample, 5 movies of 30 s were recorded using a camera level of 16. Data were analyzed with NTA Analytical Software.

Cryo-transmission electron microscopy. A total of 2–7 µl of SC EVs was deposited onto an electron microscopy grid coated with a perforated carbon film (Ted Pella, Redding, CA, USA), the excess liquid was blotted off with a filter paper, and the grid was then quickly plunged into liquid ethane. Analysis was carried out in MET Jeol 2100 (LaB6) at 80 kV.

EV marker analysis by ExoView device. A murine SC EV batch produced by the turbulence method was analysed by ExoView (NanoView Biosciences, USA). All samples were diluted in PBS with 0.05% Tween-20 (PBS-Tw). The samples were incubated on the ExoView Tetraspanin Chip for mouse EVs placed in a 24-well plate for 16 h at room temperature. The chips were washed 3 times with PBS-Tw. Chips were incubated with ExoView Tetraspanin Labelling antibodies that consist of anti-CD81 Alexa-555, anti-CD63 Alexa-488, anti-CD9

Alexa-647 and anti-calnexin Alexa 647. The antibodies were diluted 1 : 5000 in PBS-Tw with 2% BSA. The chips were incubated with 250 μL of the labelling solution for 2 h, washed in PBS-Tw and dried. The chips were imaged with the ExoView R100 reader using the ExoScan 2.5.5 acquisition software. The data were analysed using ExoViewer 2.5.0 with sizing thresholds set to 50 to 200 nm diameter.

In vitro assessment of EV pro-angiogenic properties by HUVEC scratch test

HUVEC (ATCC®) were cultured at 37 °C and 5% CO_2. DMEM supplemented with 10% FBS and 100 U mL^{-1} penicillin and 100 U mL^{-1} streptomycin was used. Cells were cultured in 150 cm^2 flasks until confluence. Pro-angiogenic properties of SC EVs were tested *in vitro* using a scratch test. Monolayers of confluent HUVEC cells in 24-well plates were scratched using a 1000 μL pipet cone and the medium was replaced by fresh one to discard detached cells. HUVEC scratched monolayers were incubated for 9 h with DMEM without serum containing SC EVs. This test was performed with an EV dose set by the producer cell/recipient cell ratio of 1 : 1, 3 : 1 or 10 : 1, corresponding to a minimum of 2.5×10^4 to a maximum of 3×10^6 EV per cell. Serum-free medium and complete medium were used as negative and positive controls, respectively. Pictures of each conditions were taken before EV incubation and 9 h later. The percentage of migration was calculated *via* the gap width between wound edges measured using Image J software at 0 and 9 h time points, 100% migration meaning total gap bridging.

Preparation of PF-127 gel. PF-127 was solubilized at a concentration of 20% (weight/weight) in PBS under agitation during 24 hours at 4 °C, followed by a sterilizing filtration (filter 0.22 μm) at 4 °C.

Characterization of PF-127 gel. Rheological studies were performed for the PF-127 hydrogels with a Physica RheoCompass MCR 302 (Anton Paar) using a cone and plate geometry (diameter = 50 mm, cone angle = 1°) and a solvent trap to prevent evaporation. The measurements of G' and G'', the elastic and viscous moduli, respectively, as a function of temperature were performed. The temperature was gradually increased by 5 °C min^{-1} starting from 5 °C to 40 °C. The sol–gel transition temperature, cross over between G' and G'', was investigated.

Rat model of colo-cutaneous fistula

All experiments were approved by the animal care and use committee in Brazil and France as well as the Ministry of Higher Education and Research in France. A surgical cecostomy communicating the cecum and the skin was performed in female 11-week old Wistar rats. The animals went through a 7-day acclimatization period with water and food *ad libitum*. The animals were housed in the laboratory animal room, in cages, with regulated temperature, ventilation, and respecting light–dark cycles. Rats received a liquid diet on the day prior to surgery and were fasted overnight before operation. Anesthesia was performed under 2% of isoflurane (Baxter, Maurepas, France). A surgical cecostomy was performed according the model described by Bültmann and colleagues.[53] Rats were placed in supine position, feet spread apart and their abdomen was shaved. After a midline laparotomy of 3 cm, the distal part of the cecum was passed with a staggered opening through the abdominal muscle and the subcutaneous space, forming a 10 mm-long tract. Four stitches (Vicryl 4/0) were used to attach the cecum to the skin at the site of the incision on the right flank of the rat, creating a colo-cutaneous fistula model. Postoperative analgesia was performed. Animals were isolated in individual cages, one animal/cage, in the pre and postoperative period. Animals were killed, after the experiment by an intracardiac injection of thiopental.

Biodistribution investigation

^{89}Zr-oxinate preparation and EV labeling for biodistribution investigation. In a first step, EVs were functionalized with the bifunctional *p*-isothiocyanatobenzyl-desferrioxamine (DFO) *via* lysine–NH_2 groups on EV outer membrane surface proteins following a protocol for antibody functionalization.[54] Briefly, a 50 mM DFO in DMSO solution was diluted 50× in pH 9 PBS. EVs were resuspended in pH 9 PBS, and centrifuged at 16 200*g* for 30 min to obtain EVs in 100 μl with a 3 mg ml^{-1} protein concentration. 3 μL of DFO solution were added to EVs, and they were incubated at 37 °C for 30 min. A final washing step (16 200*g*, 30 min, two times) with normal pH 7.4 PBS with 1% penicillin streptomycin was used to remove DFO. EVs were then frozen until use. [^{89}Zr] Zirconium[55] was produced by a ^{89}Y(p,n)^{89}Zr nuclear reaction[56,57] in a GE cyclotron PETtrace 880, using a home-made target built in aluminum. A high purity (>99%) [^{89}Y] yttrium sheet was bombarded with 12.8 MeV protons, at a 10 μA current, by 180 min. The activated ^{89}Y sheet was dissolved in 6 M HCl and [^{89}Zr]Zr^{4+} was purified by filtration in a ZR resin column (Trisken International, France) and elution was carried out with oxalate (0.1 M). A total of 100 μL of the solution was transferred to an Eppendorf tube, neutralized with 3 × 30 μL of 2 M Na_2CO_3 and incubated at 22–25 °C for 3 min, followed by the addition of 300 μL of HEPES (0.5 M pH 7.17). A total of 250 μL (130 MBq) of the solution of [^{89}Zr][Zr(ox)$_4$]$^{4-}$ was transferred to a V reaction vial containing 500 μL 8-hydroxyquinoline (8-HQ) in chloroform (1 mg mL^{-1}), and the vial was shaken for 10 min and the product [^{89}Zr][Zr(8-HQ)$_4$] was recovered from the chloroform phase by evaporation, redissolved in dimethyl sulfoxide (DMSO, 20 μL) and diluted with 0.1 mL of PBS (0.1 M pH 7.4).[58] Radiochemical purity was checked in ITLC-SG/ethyl acetate chromatography. To these vial was added 50 μL of EVs suspension (a total of 5×10^{12} EVs) and the vial was shaken for 60 min at 37 °C. This suspension was transferred to 10 kDa molecular weight cut-off filters (Amicon®Ultra – 500 μL, Merck Millipore Ltd, Ireland) and volume completed to 300 μL and centrifuged. The residual was washed twice with 300 μL of PBS, and residual ([^{89}Zr]Zr-EVs product) was removed from the Amicon®Ultra tube. The [^{89}Zr]Zr-EVs product was analysed by ITLC-SG/citrate solution (20 μM – pH 5) chromatography.

Positron emission tomography (PET)/magnetic resonance imaging (MRI) acquisition. A biodistribution study was performed in female Wistar rats (200–250 g, n = 7) purchased from the Institute of Biomedical Sciences of the University of São Paulo (ICB/USP). These rats were kept at room temperature of 22 ± 2 °C with light/dark cycle (12 : 12 h). Food and water were provided *ad libitum*. The rats were allowed to acclimatize for at least seven days. All procedures were conducted according with the guidelines of the National Council for the control of Animal Experimentation (CONCEA, Brazil) and were approved by the Ethics Committee for Animal Research of the Medical school of the University of São Paulo (CEUA-FMUSP/USP, Brazil – protocol number: 904/17). Immediately after surgical cecostomy, the animals were treated with 4 MBq of [^{89}Zr]Zr-EVs by intrafistula administration. One animal was treated with the [^{89}Zr]Zr-EVs into PF-127 gel, another with the [^{89}Zr]Zr-EVs in saline solution and a third one with the [^{89}Zr]Zr-EVs in saline intravenously, then image acquisitions were performed at 1 hour, 24 hours and 7 days.

PET/MR images were acquired with flexible knee coil MRI at the General Electric (GE) Signa PET/MR 3T (HC-FMUSP – Brazil) during the period which patients were not being attended and with all hygiene care. PET image was acquired for 15 minutes simultaneously with T1 weighted MRI with animals under anesthesia with ketamine (100 mg kg^{-1}) and xylazine (10 mg kg^{-1}). Emission sinograms were iteratively reconstructed into a single frame of 15 min (OSEM; 4 iterations and 28 subsets), after being corrected for radioactivity decay. Intra-fistula uptake of [^{89}Zr]Zr-EVs of three animals were analyzed in the PMOD 3.4 software (PMOD™ Technologies Ltd, Switzerland). Volumes of interest (VOIs) regions were drawn in the PET images fused to the T1 weighted MRI of each animal. The [^{89}Zr]Zr-EVs uptake was analyzed as a standardized uptake value (SUV), which is calculated as radioactivity concentration (kBq cc^{-1}) divided by the ratio between injected dose (kBq) and animal body weight (g) for each time point.

PET acquisition was performed to check the biodistribution of [^{89}Zr][Zr(ox)$_4$]$^{4-}$ or [^{89}Zr][Zr(DFO)] following percutaneous intra-fistula or intravenous administration after 24 hours and 7 days, as a conjugation quality control. These PET images were performed at small-animal PET scanner (Triumph™ – Gamma Medica-Ideas, Northridge, CA, USA). A static image of 25 min (5 min per bed position). Animals were anesthetized with isoflurane mixed with oxygen and 4 MBq of [^{89}Zr][Zr(ox)$_4$]$^{4-}$ or [^{89}Zr][Zr(DFO)] were injected in the tail vein. Emission sinograms were iteratively reconstructed into a single frame of 25 min (OSEM; 20 iterations and 4 subsets), after being corrected for radioactivity decay. The body temperature of the animals was maintained by heating pads and breath rate were monitored.

EV-mediated percutaneous fistula therapy in the hydrogel and follow-up

Therapy. Female Wistar rats (Janvier, 250–300 g) were randomized in three groups and treated just after cecostomy with 0.6 mL of PBS (control group, n = 8), 0.6 mL of thermoresponsive Pluronic F-127 (Sigma-Aldrich) hydrogel at 20% (gel group, n = 8) or 0.6 mL of thermoresponsive Pluronic F-127 hydrogel at 20% containing turbulence-triggered EVs at 1 × 10^{12} EVs ml^{-1} concentration (gel + EV group, n = 6). Treatment was repeated once every week during 60 days under 2% of isoflurane anesthesia. In the beginning of the study there were 8 animals per group. However, there were 2 deaths during anesthesia in the group treated with EVs plus gel.

Pre-clinical fistula therapy follow-up. Rats were weekly followed for 60 days after surgery. Animals were anesthetized using isoflurane and fistula diameter was measured by gently inserting the tip of catheters of 6; 4.5; 3; 2; 1 and 0.2 mm of diameter, from the smaller to the largest one. The presence of feces at the fistula orifice, indicative of positive fistula output, was evaluated macroscopically. The absence of feces indicated negative fistula output.

Probe-based confocal laser endomicroscopy. Microvascular network at the fistula was assessed by a probe-based confocal laser endomicroscopy device Cellvizio™ (Mauna Kea Technologies, France). This analysis was carried out at day 60th (D60), before sacrifice, under isoflurane anesthesia. The equipment featured a flexible fiber optic miniprobe that functions as a microscope objective (1.8 mm diameter, 3.5 μm spatial resolution, 12 images per second acquisition). The probe was positioned on the external fistula orifice border for image acquisition. The density of the microvascular network was investigated after the intravenous administration of FITC-dextran with an average molecular weight of 500 000 (FD500S, Sigma-Aldrich). Mosaicing™ software (Mauna Kea Technologies, France) was used for image analysis and a dedicated module, Vessel Detection™ (Mauna Kea Technologies, France), enabled to compute the functional capillary density (FCD) and diameter distribution. In order to avoid underestimating small vessels, which play an important role in tissue regeneration, we chose a diameter of interest (DOI) of 4 μm. Each parameter was evaluated on 3 different slices. In order to limit the biases related to the selection of the analysis slice, the mean of the results of 3 slices was used as a reference value for the quantitative variables.

MRI for therapy follow-up. MRI was performed using a 4.7 T preclinical MRI scanner (BioSpec 47/40 USR, Bruker, Ettlingen, Germany). MRI was carried out at D60 just before sacrifice using a T1-weighted axial and sagittal FLASH gradient-echo sequence (TR/TE: 100/2.6 ms; angle: 70°; field-of view: 5 × 5 cm; matrix: 256 × 256; resolution: 195 × 195 microns; T_{acq}: 2 min and 33 s: 11 slices of 1 mm). Animals were placed under isoflurane anesthesia and breathing was monitored. In order to facilitate imaging, a gadolinium contrast agent (Dotarem at 0.5 mM mL^{-1}, Guerbet, France) was administered *via* the external fistula orifice just before image acquisition. The first objective was to evaluate the fistula healing by measuring the area of central fistula orifice with the software, OsiriX Lite V.11.0.2, Pixmeo (Switzerland), for which the area was calculated (mm^2).

Histological analysis. At D60, rats were sacrificed and the fistula site as well as its periphery (1 cm^3 specimen) were collected and transferred to a formaline solution. Specimens were embedded in paraffin and sectioned perpendicular to the center of the fistula to obtain thin tissue sections of 7 μm, which were stained with hematoxylin and eosin (HE) and Sirius Red (fibrosis assessment). Slices were analyzed with an optical microscope (Leica DMIL). Two investigators, blinded to treatment allocation, performed histological analyses. All slides were digitally scanned (Digitiser Hamamatsu Photonics®, Massy, France) and analyzed with dedicated software (NDP.view software®, Massy, France). The density of cell type, fibrosis and inflammation were determined by semi-quantitative analysis using a score from 0 to 5. Fibrosis score (from 0 to 25) was calculated by semi-quantitative density of fibrosis (score from 0 to 5) multiplied by semi-quantitative fibroblast score (from 0 to 5). A histological scoring was used for evaluation inflammation.

Statistics

The results are presented as means ± standard deviation for continuous variables, and as percentages for categorical variables. Fischer's exact test was carried out for comparisons between categorical variables and the nonparametric Mann–Whitney test was used for non-paired continuous variables. Comparisons between more than two groups were performed with the nonparametric Kruskal–Wallis test. An estimation of the p value by the Chi-square test was carried out for the comparison concerning the number of cases per group. A *P*-value of <0.05 was considered indicative of significance. Statistical analysis was conducted using SPSS software version 24.0 (IBM Corp., Armonk, NY). GraphPadPrism (Graphpad Software, La Jolla, CA, USA) software was used for statistical analysis information displayed in figures.

Results

High-yield production of EVs in bioreactors triggered by turbulent flow

Murine SCs were cultured in 3D on the surface of microsupport beads in spinner flasks. Stirring speed in these bioreactors was tuned in order to generate a turbulent flow featuring a Kolmogorov length of 35 μm. Murine SCs were stimulated during 4 hours. Typically, this turbulence set-up may enable the production of about 500 000 EVs per cell in 4 hours while about 10 times less is produced in 48 h of starvation.[52] Herein, a total of 10^{13} murine SC EVs were obtained in 1 L bioreactors and were then isolated by ultracentrifugation and characterized by cryo-TEM, NTA and Exoview. Cryo-microscopy analysis evidenced membrane-enclosed round-shaped structures featuring high size polydispersity between 70 and 500 nm (Fig. 2A). Size distribution characteristic to EVs mainly spanning from 100 to 250 nm was observed. The values for the mean size and mode obtained by NTA were 136.2 nm and 94.8 nm, respectively, with a size distribution standard deviation of 70.4 nm (Fig. 2B and C). In more details, 90% of the particles were smaller than 228.6 nm, 50% of the particles were smaller than 112.7 nm, while 10% of the particles were smaller than 81.6 nm.

EV markers were characterized for a murine SC EV batch produced by the turbulence method *via* Exoview analysis. The obtained data indicated that the particles could be immune-captured by anti CD63 and CD81 antibodies. Minimal capture was observed by anti CD9 antibody and the same applied to negative control mouse IgG antibody (Fig. 2D). Fluorescence images enabled to visualize of single immune-captured EVs further labelled by fluorescence antibodies, especially anti CD81 (Fig. 2E). Minimal fluorescence was detected for calnexin negative cytosolic marker when using an anti-calnexin fluorescent antibody in permeabilized immune-captured EVs.

As a final formulation, EVs were combined to PF-127 hydrogel at 20% just before use. The rheological properties of PF-127 hydrogel were assessed by the evolution of dynamic storage modulus (G') and loss modulus (G'') as a function of the temperature, confirming the thermoresponsive properties of the obtained hydrogels (Fig. 2F). A transition temperature near 20 °C was determined at G′ and G'' cross over.

Cecostomy enabled the induction of a post-surgical colo-cutaneous fistula model in rats

A surgical colo-cutaneous fistula model was performed *via* a cecostomy at day 0 (Fig. 3A and B). After the surgical procedure, all fistulas featured an external orifice diameter ≥4.5 mm. Besides, all fistulas were permeable, featuring faeces secretion output, in 100% of the cases. The model allowed the formation of a communication resembling a digestive fistula-like disease with skin and intestinal lesions. The presence of a fistula tract was observed by MRI (Fig. 3C). There was no complication related to fistula induction surgery. The mean of weight before to surgery was 265.2 ± 8.3 g. Therapy follow-up after surgery was 60 days. At the end of the follow-up mean weight was 274.4 g ± 20.8 g.

Percutaneous EV delivery in the thermoresponsive gel allowed EV retention in the fistula tract

We investigated the interest of the percutaneous EV administration embedded in the thermoresponsive gel (Fig. 3D) compared to other administration strategies. A thorough biodistribution study was out of the scope of the present paper. Our aim was to appraise the potential relevance of the proposed administration strategy providing a general picture of biodistribution patterns obtained by other delivery approaches. For that, an EV radiolabeling procedure with [^{89}Zr]zirconium was conceived. The direct labelling of DFO-EVs with [^{89}Zr][Zr$(ox)_4]^{4-}$ was unsuccessful. Therefore, a [^{89}Zr][Zr$(8\text{-HQ})_4$] labelling procedure was used and this complex was obtained in 52% yield (67.6 MBq), with radiochemical purity of 97.5%. [^{89}Zr]Zr-EVs were obtained in a 32.5% yield (22 MBq) with a radiochemical purity of 89.5%. Animals were treated with [^{89}Zr]Zr-EVs *via* percutaneous intra-fistula administration in saline, percutaneous intra-fistula administration embedded in

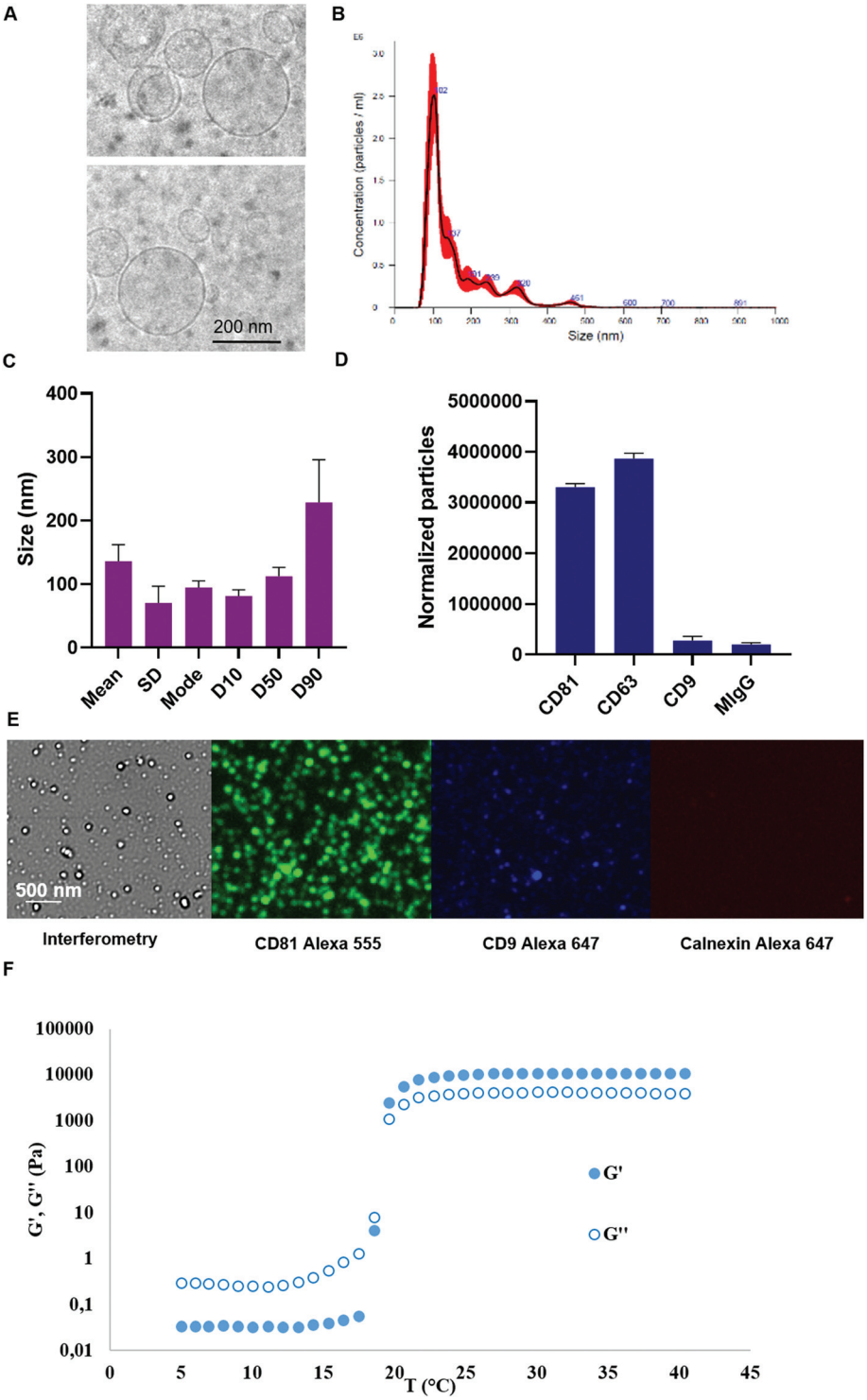

Fig. 2 Characterization of murine stem cell (SC) EVs and Pluronic F-127 hydrogel. Cryogenic transmission electron microscopy images of SC EVs (A). Size distribution of SC EVs, averaged on 5 recorded videos (B) and the mean, mode, standard deviation and percentiles of the size of EV samples, represented as the mean ± SEM of three independent batches by nanoparticle tracking analysis (C). EV marker analysis by ExoView for SC EVs using CD9, CD63 and CD81 capture antibodies with a mouse IgG2a (MIgG2a) used as negative control capture antibody (D). Representative fluorescence images of the multiplexed EV marker analysis by ExoView for SC EVs using CD81 capture antibodies. Refractometry images are shown as well as fluorescence images using CD81 and CD9 detection antibodies (positive markers) and calnexin fluorescence detection antibody (negative marker) (E). Evolution of dynamic storage modulus (G') and loss modulus (G'') of a Pluronic F-127 at 20% at a heating rate of 5 °C min^{-1} from 5 °C to 40 °C for the determination of the sol–gel transition temperature (G' and G'' cross over) (F).

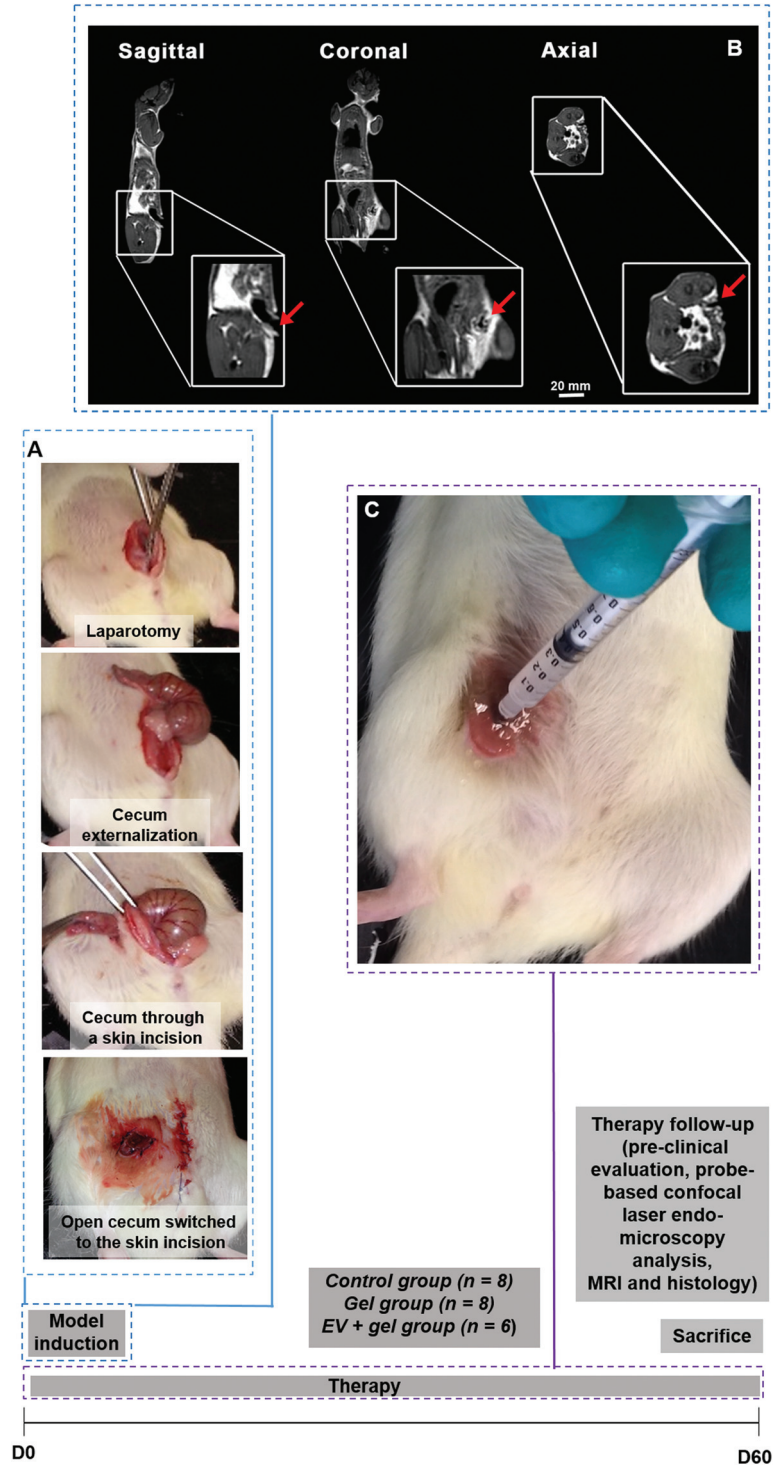

Fig. 3 Design of the *in vivo* experiments and their main steps. Study timeline and sample size per group are displayed. Surgical procedure for the colo-cutaneous fistula model induction from laparotomy to cecum communication to the skin in rats (A). T1 weighted MRI illustrating the colo-cutaneous fistula model. The red arrows indicate the fistula in different anatomical planes: sagittal, coronal, and axial (B). Percutaneous administration of the EVs into the Pluronic F-127 gel *via* the fistula external orifice (C).

the thermoresponsive gel or *via* intravenous injection in saline (Fig. 4). We observed that the percutaneous [^{89}Zr]Zr-EVs treatment in saline induced a disseminated tracer uptake in the digestive tract at 1 h. A fast decrease in the SUV of 75% in the fistula site was evidenced between 1 h and 24 h (56 and 14, respectively). Concerning the [^{89}Zr]Zr-EVs delivery percutaneously in the thermoresponsive gel, PET signal mainly remained limited to the site of interest and the SUV decrease

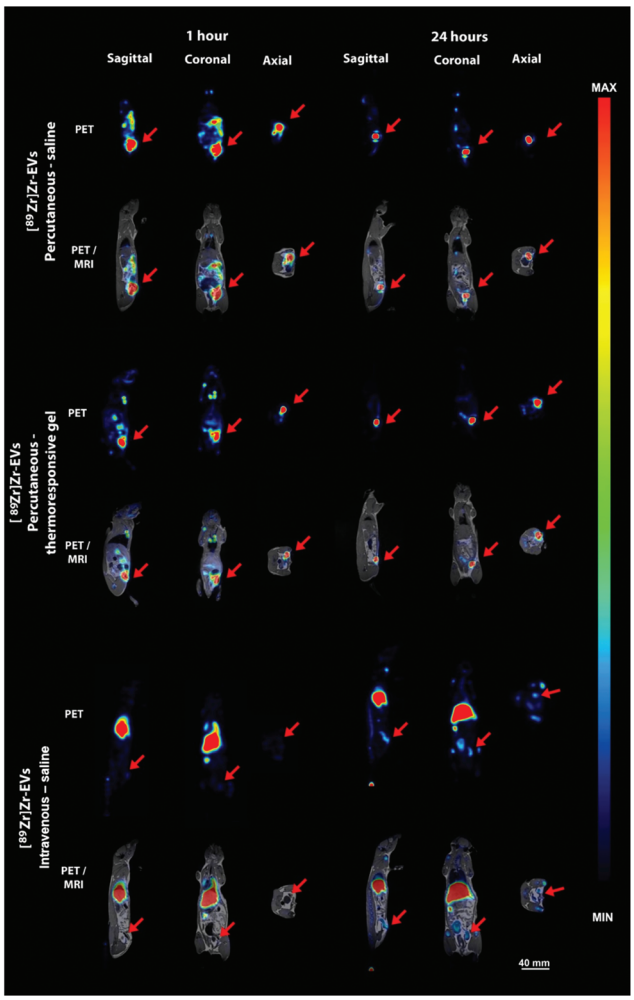

Fig. 4 PET and PET/MRI images illustrate the biodistribution and local uptake of radiotracer labeled EVs ([^{89}Zr]Zr-EVs), 1 hour and 24 hours after local percutaneous administration, in suspension or embedded in the thermoresponsive gel, or intravenous injection (3 anatomical planes are illustrated). Red arrows indicate the radiotracer uptake in the colocutaneous fistula. Note that the percutaneous treatment without gel (first line) revealed faster standardized uptake value (SUV) decrease in the fistula site, SUV mean between 1 hour and 24 hours decreased around 75%. For the percutaneous treatment with gel (middle line), the SUV at the fistula site decreased around 30% between 1 hour and 24 hours. For the intravenous injection (bottom line), there was a [^{89}Zr]Zr-EVs uptake increase of 400% between 1 hour and 24 hours. However, SUV levels were 3 times lower when compared to local percutaneous administration.

was of 30% between 1 hour and 24 hours (30 and 21, respectively). After intravenous injection, [^{89}Zr]Zr-EVs in saline mainly displayed a liver accumulation pattern along with minor uptake in the fistula site and joints. An increase of 400% was observed for the SUV in the fistula site between 1 hour and 24 hours (1.5 and 7.5, respectively) indicating EV homing. However, this SUV level were 3 times inferior when compared to local percutaneous administration. At day 7th post-administration, imaging was performed for animals treated with EVs embedded in the gel administered percutaneously or following EV intravenous injection in saline. The tracer signal was still mainly limited to the fistula site featuring a SUV decrease of just 15% compared to SUV at 24 hours for the percutaneous EV administration into the thermoresponsive gel condition (Fig. S1†). Comparatively, an almost 4-fold decrease in the SUV at the fistula site was observed for the intravenous injection condition when comparing time points 7 days and 24 hours. As control conditions, the PET biodistribution of the of the [^{89}Zr][Zr(ox)$_4$]$^{4-}$ tracer alone or linked to the conjugation [^{89}Zr][Zr(DFO)] molecule was recorded at 24 hours and 7 days after intravenous administration in saline or percutaneous administration in the thermoresponsive gel. Data showed a biodistribution pattern different from the ones observed for the [^{89}Zr]Zr-EVs (Fig. S2†). For instance, the intravenous administration of [^{89}Zr][Zr(ox)$_4$]$^{4-}$ indicated a bone biodistribution (spine) quite different for the liver biodistribution observed for the intravenous [^{89}Zr]Zr-EVs injection. This seems to indicate the effective tracer conjugation to EVs.

EV therapy in the thermoresponsive gel decreased fistula output and external orifice diameter

Repeated weekly treatment during 60 days with the gel or the gel with EVs was well tolerated by animals. No evident signs of local irritation, allergy or toxicity were observed. No statistically significant difference in mean body weight was evidenced for animals in the control, gel and EVs + gel group at day 60th after the begin of the therapy (Fig. S3†). Fistula output was evaluated at day 30th. One case of no fistula output (absence of faeces secretion) from 8 animals was observed for the control and also for the gel group, corresponding to 12.5%, for both. Two cases of no fistula output from 6 animals were observed for the group treated with EVs and gel, corresponding to 33% of the animals (Fig. S4†). Fistula closure, output and external orifice diameter were evaluated at day 60th. One case of fistula closure per group was observed for each group, corresponding to 12.5%; 12.5% and 16.7% of the cases for the control, gel and EVs + gel groups. The frequency of no fistula output was significantly different when comparing the control group (1 case from 8: 12.5% of the animals) to the EVs + gel group (4 cases from 6: 66.7% of the animals) (Fig. 5A). No significant difference was observed when comparing the frequency of no output for the control group to the gel one (2 from 8 cases: 25% of the animals) nor the gel group to the EVs + gel one. The external orifice diameter distribution showed a clear shift towards smaller size ranges. The size of external orifice diameter ranges increased in the following sequence EVs + gel < gel < control animals (Fig. S5†). The frequency of fistulas featuring an external orifice diameter <3 mm was significantly different when comparing the control group (1 case from 8: 12.5% of the animals) to the EVs + gel one (4 cases from 6: 66.7% of the animals). No significant difference in the frequency of fistulas featuring an external orifice diameter <3 mm was observed when comparing the control group and the gel one (3 cases from 8: 37.5% of the animals) nor the gel group to the EVs + gel one (Fig. 5B). The macroscopic view of the fistulas revealed a higher and

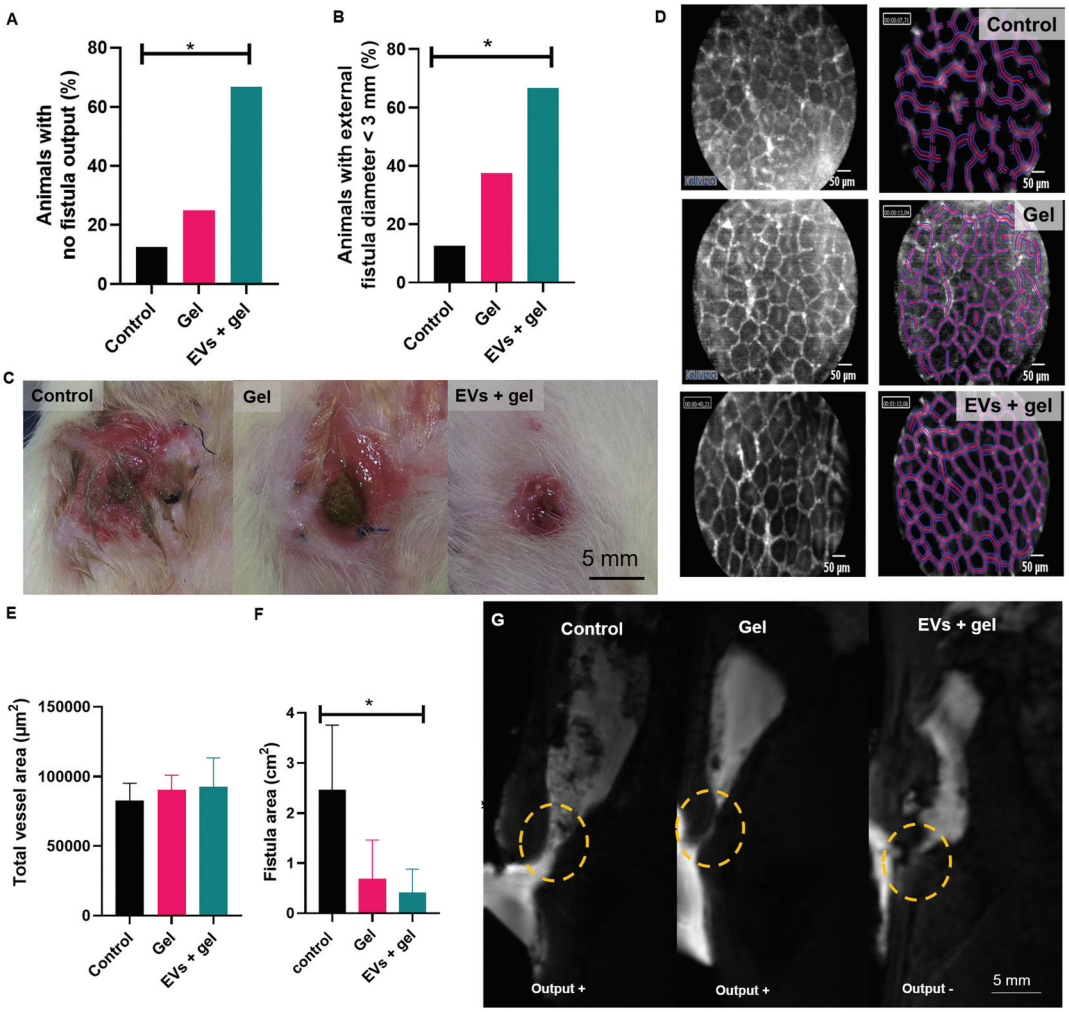

Fig. 5 Potency evaluation *in vivo* by a multi-modal approach in rats treated with the gel or EVs + gel in comparison to an untreated negative control. Preclinical evaluation of fistulas at day 60 indicating the percentage of animals per group featuring the absence of faeces (no output) at the external fistula orifice (A) as well as percentage of animals per group featuring an external orifice diameter inferior to 3 mm (B). For both A and B, *p* values were estimated by Chi-square test based on the number of cases per group featuring the presence (output+) or absence of feces (output–) at the external fistula orifice (A) and number of cases featuring an external orifice diameter inferior or superior to 3 mm (B). Macroscopic aspect of external fistula orifices at day 60 for the three groups (C). Therapy follow-up by probe-based confocal laser *endo*-microscopy analysis at day 60 showing vessel network (D) and the quantification of total vessel area (E) for each group. Therapy follow-up by MRI analysis at day 60 showing fistula area quantification (F) and representative related images (G) for each group (fistula tracts were indicated by yellow dotted circles). For both E and F, *p* values were computed using Mann Whitney test.

extended zone featuring an inflammatory aspect surrounding the external orifice for control and gel groups in comparison to fistulas from the EVs + gel group (Fig. 5C).

EV therapy in the thermoresponsive gel seemed to improve vascularization while reducing fistula area: an image-based therapy follow-up

Vascularization parameters were analysed by probe-based confocal laser endomicroscopy. No significant difference was observed for group comparison in terms of vessel diameter, total vessel length, total vessel area, mean vessel diameter nor functional capillary density length, for instance (Table S1†). There was a trend towards a higher functional capillary density area and total vessel area for animals from the group gel or EVs + gel one in comparison to control (Fig. 5D, E and Table S1†). This trend did not reach statistical significance probably due to the reduced sample size.

Fistula metrics was assessed by MRI analysis right after the percutaneous injection of a gadolinium contrast agent *via* the external fistula orifice at day D60. There was a trend towards a reduced fistula length when comparing EVs + gel group to control (Table S2†). MRI data evidenced a significant reduction of the fistula area when comparing EVs + gel group to control (Fig. 5F and G). No significant reduction of the fistula area was observed when comparing the gel group to control nor the gel group to the EVs + gel one.

Histological analysis indicated a decrease in inflammation and fibrosis and an increase in neo-vessel density induced by EV therapy in the thermoresponsive gel

Histological analysis was carried out to accesses inflammation, fibrosis and vascularization. A histology score (integrating epithelial damage, mucosal inflammation and submucosal inflammation parameters as indicated in the Table S3†) evidenced a significant difference when comparing the control group to the EVs + gel one (Fig. 6A). A significant difference was also observed when comparing the gel group and EVs + gel one. Accordingly, the density of polynuclear neutrophils (PNN) was significantly lower for the EVs + gel group than observed for the control one (Fig. 6B). The histological evaluation validated the trend observed by probe-based confocal laser endomicroscopy as the density of neo-vessel score was significantly higher for the EVs + gel group in comparison to control (Fig. 5C). This is also in agreement with *in vitro* pro-angiogenic (pro-migratory) properties of the EVs (Fig. S6†). A significant reduction in the fibrosis score was also evidenced when comparing the EVs + gel group to the control one (Fig. 6D). Besides, a significant difference in the fibrosis score was also observed when comparing the gel group and the EVs + gel one. Extensive fibrosis and mucosa damage was observed for the control group (Fig. 6E). Fibrosis and mucosa damage seemed more limited in the gel group (Fig. 6F). Fibrosis was limited in the gel and EVs + gel group, which featured minimal mucosa damage (Fig. 6G). Table S4† provides additional histology data.

Discussion

Herein we investigated a biomaterial-based cell-free local therapy for post-surgical fistulas. This combined therapy relied on turbulence SC EVs embedded in a PF-127 thermoresponsive hydrogel administered percutaneously in colo-cutaneous fistulas.

As far as we know, this is the first time that SC-EVs incorporated in a thermoresponsive hydrogel are investigated for the therapy of post-surgical colo-cutaneous fistulas as an alternative to cell therapy. In a previous report from our team, SC organized in double cell sheets showed a therapeutic effect in an equivalent fistula model in mice.[59] In the attempt to shed light on the mechanisms of cell therapy for fistula treatment, our group performed *in vivo* experiments with doubled labelled SCs for fluorescence and MRI tracking. SC detection at fistula site was showed just following transplantation, but it could not be clearly evidenced 7 and 14 days post-treatment. We showed that SC cell sheet therapeutic benefits on fistula healing were accompanied by a paracrine effect with an increase in the expression of anti-inflammatory cytokines and intestinal growth factors involved in tissue repair.[59]

As EVs are known to participate in SC paracrine role,[1,2] we decided to test herein an EV-based cell free therapy. SC EVs were produced *via* a high-yield scalable strategy in bioreactors. The turbulence method in 4 h may enable up to a 10-fold increase in EV production yield compared the state-of-the-art starvation approach in 48 h.[52] Our turbulence strategy is fully integrated to the cell culture in stirred tank in cGMP bioreactors. We evidenced that the turbulence approach was scalable based on turbulence physical laws *via* the Kolmogorov equation.[52] The choice of the turbulence approach enabling high-yield, scalability and cGMP compliance is one of the translational strengths of our investigation. The comparison between turbulence SC EVs and state-of-the-art ones in terms of properties and potency *in vitro* is provided elsewhere.[52]

Turbulence SC EVs were combined to PF-127 thermoresponsive hydrogel for local colo-cutaneous fistula therapy. The aim of the hydrogel was two-fold: (i) to act as a sealant promoting fistula mechanical occlusion and (ii) to constitute a delivery system for EVs modulating their release and biodistribution. Concerning fistula sealants, other biomaterials such as porcine plug or fibrin glue[60] have been investigated in a clinical setting for post-surgical fistula therapy. However, the use of these biomaterials may be limited by abscess formation[61] and spontaneous expulsion.[62] We have recently evidenced in a case report that PF-127 gel may be a thermo-actuated fistula sealant of interest. It was well-tolerated by the patient while inducing a reduction in the external fistula orifice diameter and secretion output volume in combination to a stent placement.[63] Due to its thermoresponsive properties, this biomaterial can be administrated as a liquid *via* a catheter. Its gelation *in situ* at body temperature is expected to enable its retention at the fistula tract, limiting the circulation of secretions and thus favoring the healing process.

As we have mentioned, the use of the PF-127 gel herein goes beyond a sealant agent also providing a delivery system for EV administration locally in the rat model of colo-cutaneous post-surgical fistula. In this regard, we developed an EV labelling strategy with a radiotracer in order to identify the biodistribution pattern of EVs following their administration either percutaneously in the gel or in saline in comparison to an intravenous administration in saline. We selected [^{89}Zr]zirconium as the radionuclide as its half-life of 3.3 days enables the *in vivo* tracking from hours to days post administration. EVs were tagged with [^{89}Zr]zirconium *via* a double labelling strategy. In a first attempt, we investigated EV labelling by the direct reaction between DFO-EVs[54] with [^{89}Zr][Zr(ox)$_4$]$^{4-}$. This strategy was not successful. Therefore, we decided to use [^{89}Zr][Zr(8-HQ)$_4$] to react with DFO-EVs which could concurrently (i) transfer part of the $^{89}Zr^{4+}$ to the DFO bounded to EVs or (ii) cross the lipid membrane delivering $^{89}Zr^{4+}$ into the EV inner compartment. Control experiments showed that the biodistribution of [^{89}Zr][Zr(ox)$_4$]$^{4-}$ or [^{89}Zr][Zr(DFO)] was quite distinct from the one observed for [^{89}Zr]Zr-EVs. This supports the assumption of a successful EV radiolabeling by our proposed double strategy. As far as we know, this is the first time that EVs are tagged with [^{89}Zr]zirconium *via* this double labelling strategy, which allowed tracking up to 7 days post-administration. For instance, different EV radiolabelling strategies with [^{99}mTc]Tc[64] or [^{124}I]I[65] were reported in the literature with a tracking time up to and 5 h and 72 h, respectively.

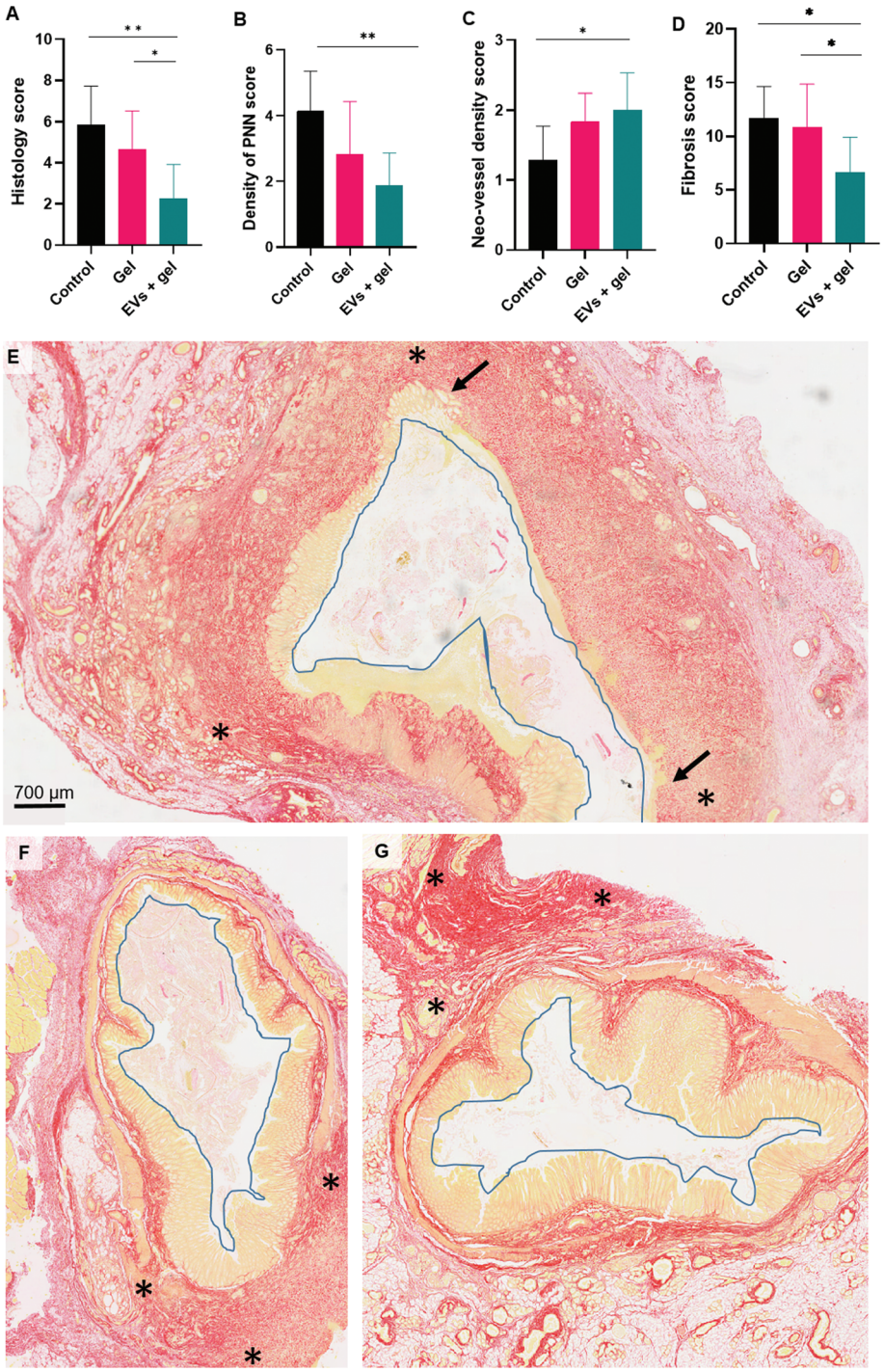

Fig. 6 Potency evaluation *in vivo* by histology in rats treated with the gel or EVs + gel in comparison to an untreated negative control. Therapy follow-up for the three groups by histological analysis at day 60 assessing a histology score based on epithelial damage, mucosal inflammation and submucosal inflammation parameters (A). Therapy follow-up for the three groups by histological analysis at day 60 assessing the polynuclear neutrophils (PNN) density (B), neo-vessel density (C) and fibrosis (D) scores. Mann Whitney test was used for computing p values in group comparison for all scores. Histology analysis (Sirius red staining) of the colo-cutaneous fistulas from control (E), gel (F) and EVs + gel (G) groups. Note that the fistula orifice was delineated in blue color and main fibrosis regions, in red staining, were delimitated by *. The epithelium was identified by an orange staining. Important epithelial damage was observed for the control group and its extent was indicated by black arrows.

By using the [^{89}Zr]Zr-EVs, we observed that the highest SUV at the fistula region were obtained following percutaneous administration. Besides, signal detection was mainly restrained to the site of interest when administration was performed percutaneously *via* the thermoresponsive hydrogel. Signal persisted with a 30% reduction in 7 days. In a related

literature approach, a pH-responsive hydrogel featuring immediate gelation upon administration into physiological systems was investigated for local EV delivery. A sustained EV delivery until day 4 post-administration was observed with EV localization in the tissue surrounding the injection site.[66] In a myocardial infarction model disease, it was reported that SC EV local delivery in the heart of rats *via* an alginate hydrogel improved EV cardiac retention.[67] *Ex vivo* 2D optical microscopy coupled to 3D optical tomography revealed a stronger fluorescent signal from DiR-labeled EVs for animals treated with in EVs incorporated in the gel compared to those treated with EVs alone.

Considering the potential interest of local percutaneous EV administration in the PF-127 hydrogel indicated by our biodistribution data, we next evaluated the therapeutic outcome of this strategy in colo-cutaneous fistulas.

The combination of EVs and PF-127 gel biomaterial was previously tested in the therapy of post-surgical oesophageal fistulas in pigs by our team.[68] Of note, a different producer cell type (primary AdSCs) was used in the precedent study. In this preceding investigation, we showed by rheological analysis that the dispersion of EVs into PF-127 gel did not impact its thermoresponsive properties. EV integration into the gel also seemed to have minor impact on EV integrity. We evidenced that EV release was expected to be driven by the saliva flow exerting a dilution effect on the gel. Indeed, we showed that the aqueous dilution of the gel to a concentration inferior to 13% notably induced a viscosity decrease and the release of EVs.[68] Based on these data, we chose the PF-127 concentration of 20%. In principle, we could choose any concentration ≥14%. However, at 14% there would be a transition to a liquid state releasing the EVs even at a minimal dilution, resulting in a burst EV release. We chose a concentration superior to this in order to enable the gel to withstand to a dilution factor of about 1.5 before transition to a liquid state to allow EV release in a more sustained way.

In our previous study, an anti-inflammatory, anti-fibrotic and pro-angiogenic effect was observed for animals treated with EVs embedded in the PF-127 hydrogel with total fistula healing being observed in this pig esophagocutaneous disease model.[68] Considering the differences in fistula tract size and secretion constitution/volume, the EV release and fate as well as the therapeutic outcome following the administration of EVs and PF-127 gel biomaterial in a colo-cutaneous fistula in rats may be indeed distinct from the one observed in the esophagocutaneous fistulas in pigs. Importantly, gel dilution factor is expected to be reduced in the colo-cutaneous model as the faeces secretion features inferior aqueous constitution in comparison to the saliva secretion in the oesophagus. The smaller fistula tract size in the colo-cutaneous rat model in comparison to the esophagocutaneous fistula model in pigs is expected to influence the gel residence time as the "reservoir" volume of these tracts are different. In brief, the combined EV/biomaterial fate and the obtained therapeutic outcome may be influenced by fistula characteristics, which depend on the involved organs. Despite these differences, we observed a therapeutic effect following the percutaneous EV administration in the gel for both the colo-cutaneous model and the esophagocutaneous one. The investigation of our approach in different fistula settings is of interest in order to extend the clinical relevance of the local delivery of EVs in the PF-127 thermoresponsive hydrogel.

Conclusions

Intestinal fistulas secondary to surgery are a major health problem. Current unmet needs require innovative strategies. We evidenced here the therapeutic potential of a biomaterial-based cell-free local EV therapy for the management of colo-cutaneous post-surgical fistulas. Thanks to a turbulence flow stimulation, EVs were produced in high-yield in an approach that combines scalability and cGMP capabilities, which is a translational asset of our study. EVs were tagged with [^{89}Zr]zirconium *via* a double labelling strategy, which allowed tracking up to 7 days post-administration. This radiolabeling approach enabled us to identify the pattern of EV biodistribution following intravenous injection in saline in comparison to percutaneous administration in saline or PF-127 gel in a colo-cutaneous fistula model in rats. We observed that the highest EV retention at the fistula site was observed following percutaneous administration. Besides, fistula retention of EVs was more prominent when their percutaneous administration was performed embedded in the thermoresponsive hydrogel. We assessed therapy outcome following the latter administration strategy by evaluating fistula output and external orifice diameter by pre-clinical macroscopic analysis; vascularization by probe-based confocal laser endomicroscopy and fistula metrics by MRI. Histology was equally assessed. Based on this multi-modal approach, we evidenced that the local administration of SC EVs in the thermoresponsive hydrogel reduced colo-cutaneous fistula external diameter, area, output, fibrosis and inflammation while increasing the density of neo-vessels in comparison to the negative PBS control. Altogether, our study brings prospects for a local minimally-invasive EV delivery relying on a thermo-actuated administration strategy in PF-127 gel in colo-cutaneous fistulas. Importantly, PF-127 gel has been previously approved for clinical use (Legoo, Genzyme), which may facilitate the clinical translation of our approach. This study extends insights from a previous investigation of our team that showed successful post-surgical esophagocutaneous fistula therapy by the equivalent strategy. As a future perspective, additional Crohn's disease and post-surgical fistula models involving different digestive organs should be also investigated to appraise post-surgical fistula disease heterogeneity. Hopefully, these further studies may confirm the versatile potential of the proposed approach as a next-generation therapeutic option for digestive fistula management in a "one-fits-all" basis. The translational assets of the proposed strategy may accelerate and render economically feasible pharmaceutical development steps toward clinical investi-

gation in the perspective to tackle unmet needs and benefit patient care.

Author contributions

Conception, design, and study supervision: Amanda Karine Andriola Silva, Gabriel Rahmi, Florence Gazeau. Acquisition of data: Max Piffoux, Alba Nicolás-Boluda, Arthur Berger, Alice Grangier, Imane Boucenna, Caroline Cristiano Real, Fabio Luiz Navarro Marques, Daniele de Paula Faria, Amália Cinthia Meneses do Rego, Chloe Broudin, Analysis and interpretation of data: Arthur Berger, Olivier Clément, Christophe Cellier, Carlos Alberto Buchpiguel; Writing, review, and/or revision of the manuscript: Amanda Karine Andriola Silva, Gabriel Rahmi, Claire Wilhelm, Florence Gazeau, Arthur Berger

Conflicts of interest

Florence Gazeau, Amanda Karine Andriola Silva, Claire Wilhelm and Gabriel Rahmi are co-founders of the spin-off Evora Biosciences. Amanda Karine Andriola Silva, Claire Wilhelm are co-founders of the spin-off EverZom. The other authors are no conflicts to declare.

Acknowledgements

This work was funded by the French National Agency for Research (ANR, Fisther project) and by IDEX Université de Paris. We would like to thank Monica Joana Kan Golcman for technical assistance at FMUSP. CCR was a postdoctoral fellowship from GE Healthcare – Brazil (grant #104.441). The authors thank Gwennhael Autret and the Small Animal Imaging Platform Paris – Descartes PARCC-HEGP for MRI. The authors also thank Dr Guillaume Perrod for assistance in probe-based confocal laser endomicroscopy experiments. We acknowledge Dr Alexandra Shephard (Nanoview, UK) for Exoview analysis. We thank Professor Roger Chammas for fruitful discussions.

References

1 X. Liang, Y. Ding, Y. Zhang, H.-F. Tse and Q. Lian, *Cell Transplant.*, 2014, **23**, 1045–1059.
2 R. C. Lai, F. Arslan, M. M. Lee, N. S. K. Sze, A. Choo, T. S. Chen, M. Salto-Tellez, L. Timmers, C. N. Lee, R. M. El Oakley, G. Pasterkamp, D. P. V. de Kleijn and S. K. Lim, *Stem Cell Res.*, 2010, **4**, 214–222.
3 B. Hugel, M. C. Martinez, C. Kunzelmann and J. M. Freyssinet, *Physiology*, 2005, **20**, 22–27.
4 J. Ratajczak, M. Wysoczynski, F. Hayek, A. Janowska-Wieczorek and M. Z. Ratajczak, *Leukemia*, 2006, **20**, 1487–1495.
5 G. Camussi, M. C. Deregibus, S. Bruno, V. Cantaluppi and L. Biancone, *Kidney Int.*, 2010, **78**, 838–848.
6 H. Xin, Y. Li, Y. Cui, J. J. Yang, Z. G. Zhang and M. Chopp, *J. Cereb. Blood Flow Metab.*, 2013, **33**, 1711–1715.
7 L. A. Reis, F. T. Borges, M. J. Simoes, A. A. Borges, R. Sinigaglia-Coimbra and N. Schor, *PLoS One*, 2012, **7**, e44092.
8 Y. Zhou, H. Xu, W. Xu, B. Wang, H. Wu, Y. Tao, B. Zhang, M. Wang, F. Mao and Y. Yan, *Stem Cell Res. Ther.*, 2013, **4**, 1–13.
9 B. Zhang, M. Wang, A. Gong, X. Zhang, X. Wu, Y. Zhu, H. Shi, L. Wu, W. Zhu and H. Qian, *Stem Cells*, 2015, **33**, 2158–2168.
10 C. Y. Tan, R. C. Lai, W. Wong, Y. Y. Dan, S.-K. Lim and H. K. Ho, *Stem Cell Res. Ther.*, 2014, **5**, 76.
11 M. Herrera, V. Fonsato, S. Gatti, M. Deregibus, A. Sordi, D. Cantarella, R. Calogero, B. Bussolati, C. Tetta and G. Camussi, *J. Cell. Mol. Med.*, 2010, **14**, 1605–1618.
12 T. Li, Y. Yan, B. Wang, H. Qian, X. Zhang, L. Shen, M. Wang, Y. Zhou, W. Zhu and W. Li, *Stem Cells Dev.*, 2012, **22**, 845–854.
13 S. Gatti, S. Bruno, M. C. Deregibus, A. Sordi, V. Cantaluppi, C. Tetta and G. Camussi, *Nephrol., Dial., Transplant.*, 2011, **26**, 1474–1483.
14 L. Hu, J. Wang, X. Zhou, Z. Xiong, J. Zhao, R. Yu, F. Huang, H. Zhang and L. Chen, *Sci. Rep.*, 2016, **6**, 32993.
15 J. Zhang, J. Guan, X. Niu, G. Hu, S. Guo, Q. Li, Z. Xie, C. Zhang and Y. Wang, *J. Transl. Med.*, 2015, **13**, 49.
16 T. Furuta, S. Miyaki, H. Ishitobi, T. Ogura, Y. Kato, N. Kamei, K. Miyado, Y. Higashi and M. Ochi, *Stem Cells Transl. Med.*, 2016, **5**, 1620–1630.
17 S. El Andaloussi, I. Mäger, X. O. Breakefield and M. J. Wood, *Nat. Rev. Drug Discovery*, 2013, **12**, 347–357.
18 R. C. Lai, T. S. Chen and S. K. Lim, *Regener. Med.*, 2011, **6**, 481–492.
19 B. Zhang, R. Yeo, K. Tan and S. Lim, *Int. J. Mol. Sci.*, 2016, **17**, 174.
20 R. W. Y. Yeo, R. C. Lai, K. H. Tan and S. K. Lim, *Exosomes Microvesicles*, 2013, **1**, 1–12.
21 P. Vader, E. A. Mol, G. Pasterkamp and R. M. Schiffelers, *Adv. Drug Delivery Rev.*, 2016, **106**, 148–156.
22 T. Imai, Y. Takahashi, M. Nishikawa, K. Kato, M. Morishita, T. Yamashita, A. Matsumoto, C. Charoenviriyakul and Y. Takakura, *J. Extracell. Vesicles*, 2015, **4**, 26238.
23 S. Bala, T. Csak, F. Momen-Heravi, D. Lippai, K. Kodys, D. Catalano, A. Satishchandran, V. Ambros and G. Szabo, *Sci. Rep.*, 2015, **5**, 10721.
24 B. György, M. E. Hung, X. O. Breakefield and J. N. Leonard, *Annu. Rev. Pharmacol. Toxicol.*, 2015, **55**, 439–464.
25 A. Fuster-Matanzo, F. Gessler, T. Leonardi, N. Iraci and S. Pluchino, *Stem Cell Res. Ther.*, 2015, **6**, 227.
26 J. Malda, J. Boere, C. H. Van De Lest, P. R. Van Weeren and M. H. Wauben, *Nat. Rev. Rheumatol.*, 2016, **12**, 243.
27 X. Liu, Y. Yang, Y. Li, X. Niu, B. Zhao, Y. Wang, C. Bao, Z. Xie, Q. Lin and L. Zhu, *Nanoscale*, 2017, **9**, 4430–4438.

28 J. D. Kretlow, L. Klouda and A. G. Mikos, *Adv. Drug Delivery Rev.*, 2007, **59**, 263–273.
29 L. Klouda, *Eur. J. Pharm. Biopharm.*, 2015, **97**, 338–349.
30 M. R. Matanović, J. Kristl and P. A. Grabnar, *Int. J. Pharm.*, 2014, **472**, 262–275.
31 M. Quinn, S. Falconer and R. F. McKee, *World J. Surg.*, 2017, **41**, 2502–2511.
32 D. Lloyd, S. Gabe and A. Windsor, *Br. J. Surg.*, 2006, **93**, 1045–1055.
33 L. J. Williams, S. Zolfaghari and R. P. Boushey, *Clin. Colon Rectal Surg.*, 2010, **23**, 209–220.
34 N. Kumar and C. C. Thompson, *Gastrointest. Endosc. Clin. N. Am.*, 2013, **23**, 123–136.
35 A. Swaminath, R. Taunk and G. Lawlor, *World J. Gastrointest. Pharmacol. Ther.*, 2014, **5**, 113–121.
36 A. Kontzias, A. Kotlyar, A. Laurence, P. Changelian and J. J. O'Shea, *Curr. Opin. Pharmacol.*, 2012, **12**, 464–470.
37 F. E. E. de Vries, J. J. Atema, O. van Ruler, C. J. Vaizey, M. J. Serlie and M. A. Boermeester, *World J. Surg.*, 2017, **17**, 4224.
38 E. Girard, M. Messager, A. Sauvanet, S. Benoist, G. Piessen, J. Y. Mabrut and C. Mariette, *J. Visc. Surg.*, 2014, **151**, 441–450.
39 J. Hammond, S. Lim, Y. Wan, X. Gao and A. Patkar, *J. Gastrointest. Surg.*, 2014, **18**, 1176–1185.
40 G. Galloro, S. Ruggiero, T. Russo, D. A. Telesca, M. Musella, M. Milone and R. Manta, *World J. Gastrointest. Endosc.*, 2015, **7**, 843–846.
41 T. P. Kingham and H. L. Pachter, *J. Am. Coll. Surg.*, 2009, **208**, 269–278.
42 Y. Kulu, M. W. Büchler and A. Ulrich, *Chirurgie*, 2015, **86**, 311–318.
43 A. Baruah, L. M. W. Kee Song and N. S. Buttar, *Tech. Gastrointest. Endosc.*, 2015, **17**, 178–188.
44 I. Araújo-Filho, A. C. M. Rêgo and F. I. Pinheiro, *Indian J. Med. Res. Pharm. Sci.*, 2016, **3**, 36–47.
45 N. Kumar and C. C. Thompson, *Gastrointest. Endosc. Clin.*, 2013, **23**, 123–136.
46 G. Mauri, L. C. Pescatori, C. Mattiuz, D. Poretti, V. Pedicini, F. Melchiorre, U. Rossi, L. Solbiati and L. M. Sconfienza, *Radiol. Med.*, 2017, **122**, 88–94.
47 J. Galipeau and L. Sensébé, *Cell Stem Cell*, 2018, **22**, 824–833.
48 C. Sheridan, *Nat. Biotechnol.*, 2018, **36**, 212.
49 S. M. Aldaqal, M. F. Khayat, R. Y. Bokhary, M. M. Wakka, A. A. Merdad and L. A. Merdad, *Int. Surg.*, 2015, **100**, 748–754.
50 P. Sukho, G. S. A. Boersema, A. Cohen, N. Kops, J. F. Lange, J. Kirpensteijn, J. W. Hesselink, Y. M. Bastiaansen-Jenniskens and F. Verseijden, *Biomaterials*, 2017, **140**, 69–78.
51 P. Sukho, G. S. Boersema, N. Kops, J. F. Lange, J. Kirpensteijn, J. W. Hesselink, Y. M. Bastiaansen-Jenniskens and F. Verseijden, *J. Visualized Exp.*, 2018, e57213.
52 M. Piffoux, A. K. A. Silva, O.-W. Merten and C. Wilhelm and F. Gazeau, WO/2019/002608, 2019.
53 O. Bültmann, C. Philipp, M. Ladeburg and H.-P. Berlien, *Res. Exp. Med.*, 1998, **198**, 215–228.
54 M. J. Vosjan, L. R. Perk, G. W. Visser, M. Budde, P. Jurek, G. E. Kiefer and G. A. Van Dongen, *Nat. Protoc.*, 2010, **5**, 739–743.
55 H. H. Coenen, A. D. Gee, M. Adam, G. Antoni, C. S. Cutler, Y. Fujibayashi, J. M. Jeong, R. H. Mach, T. L. Mindt and V. W. Pike, *Nucl. Med. Biol.*, 2017, **55**, v–xi.
56 S. L. Queern, T. A. Aweda, A. V. F. Massicano, N. A. Clanton, R. El Sayed, J. A. Sader, A. Zyuzin and S. E. Lapi, *Nucl. Med. Biol.*, 2017, **50**, 11–16.
57 P. Charoenphun, L. K. Meszaros, K. Chuamsaamarkkee, E. Sharif-Paghaleh, J. R. Ballinger, T. J. Ferris, M. J. Went, G. E. Mullen and P. J. Blower, *Eur. J. Nucl. Med. Mol. Imaging*, 2015, **42**, 278–287.
58 N. Li, Z. Yu, T. T. Pham, P. J. Blower and R. Yan, *Int. J. Nanomed.*, 2017, **12**, 3281.
59 G. Rahmi, L. Pidial, A. K. A. Silva, E. Blondiaux, B. Meresse, F. Gazeau, G. Autret, D. Balvay, C. A. Cuenod, S. Perretta, B. Tavitian, C. Wilhelm, C. Cellier and O. Clément, *Theranostics*, 2016, **6**, 739–751.
60 J. Avalos-González, E. Portilla-deBuen, C. A. Leal-Cortés, A. Orozco-Mosqueda, M. del Carmen Estrada-Aguilar, G. A. Velázquez-Ramírez, G. Ambriz-González, C. Fuentes-Orozco, A. E. Guzmán-Gurrola and A. González-Ojeda, *World J. Gastroenterol.*, 2010, **16**, 2793.
61 G. Buchanan, C. Bartram, R. S. Phillips, S. T. Gould, S. Halligan, T. Rockall, P. Sibbons and R. Cohen, *Dis. Colon Rectum*, 2003, **46**, 1167–1174.
62 S. Amrani, A. Zimmern, K. O'Hara and M. Corman, *Gastroenterol. Clin. Biol.*, 2008, **32**, 946–948.
63 A. Berger, E. Caudron, G. Perrod, I. Boucenna, F. Gazeau, C. Wilhelm, A. Berger, O. Clément, C. Cellier, A. K. A. Silva and G. Rahmi, *Clinics and Research in Hepatology and Gastroenterology*, DOI: 10.1016/j.clinre.2020.06.001.
64 D. W. Hwang, H. Choi, S. C. Jang, M. Y. Yoo, J. Y. Park, N. E. Choi, H. J. Oh, S. Ha, Y.-S. Lee, J. M. Jeong, Y. S. Gho and D. S. Lee, *Sci. Rep.*, 2015, **5**, 15636.
65 F. Royo, U. Cossío, A. Ruiz de Angulo, J. Llop and J. M. Falcon-Perez, *Nanoscale*, 2019, **11**, 1531–1537.
66 E. A. Mol, Z. Lei, M. T. Roefs, M. H. Bakker, M. J. Goumans, P. A. Doevendans, P. Y. Dankers, P. Vader and J. P. Sluijter, *Adv. Healthcare Mater.*, 2019, **8**, 1900847.
67 K. Lv, Q. Li, L. Zhang, Y. Wang, Z. Zhong, J. Zhao, X. Lin, J. Wang, K. Zhu, C. Xiao, C. Ke, S. Zhong, X. Wu, J. Chen, H. Yu, W. Zhu, X. Li, B. Wang, R. Tang, J. A. Wang, J. Huang and X. Hu, *Theranostics*, 2019, **9**, 7403–7416.
68 A. K. Silva, S. Perretta, G. Perrod, L. Pidial, V. Lindner, F. Carn, S. Lemieux, D. Alloyeau, I. Boucenna and P. Menasché, *ACS Nano*, 2018, **12**, 9800–9814.